International Forum on Aeroelasticity and Structural Dynamics
IFASD 2024
17-21 June 2024, The Hague, The Netherlands

WIND TUNNEL TESTING AND MODAL VALIDATION OF TU-FLEX'S HIGH ASPECT-RATIO WINGS

Pedro J. González[1], Guilherme C. Barbosa[1], Álvaro A. G. Quesada[1], Gerrit Stavorinus[1], Flávio J. Silvestre[1], Jonathan Hilger[2], Charlotte Hanke[2], Arne Voß[2], and Wolf R. Krüger[2]

[1]Technical University of Berlin
Marchstraße 12, 10587 Berlin, Germany
p.gonzalez.ramirez@tu-berlin.de
g.chaves.barbosa@tu-berlin.de
garcia.quesada@campus.tu-berlin.de
gerrit.s.stavorinus@campus.tu-berlin.de
flavio.silvestre@tu-berlin.de

[2]DLR, German Aerospace Center,
Bunsenstraße 10, 37073 Göttingen, Germany
Jonathan.Hilger@dlr.de
Charlotte.Hanke@dlr.de
Arne.Voß@dlr.de
Wolf.Krueger@dlr.de

Keywords: High Aspect Ratio, Wind Tunnel Test, GVT, Model Validation

Abstract: High aspect ratio flexible wing aircraft present very complex and coupled structural and flight dynamics. This research describes a bottom-to-top validation process for this type of wing. This procedure starts with static, followed by ground vibration and wind tunnel tests. The concept of this approach is to first validate the structural and aeroelastic models before addressing the full flying vehicle. The experimental data was used to tune the structural model of a flexible flying demonstrator called TU-Flex. This aircraft was designed as a flying lab capable of recording coupled flight dynamic data of a flexible aircraft with a transport/airliner configuration. Three software were used to design the wing and to define the experimental test cases: NASTRAN, Loads Kernel, and ModSiG. The gathered data permitted tuning and showing the accuracy of the structural model. It also allows for finding inaccuracies in the aerodynamic and aeroelastic models for further tuning. The models are capable of capturing the overall aeroelastic trend nevertheless, fine tuning is now necessary. Therefore, the proposed process seems adequate to collect all necessary data to tune aeroelastic models within the process to prepare the models for the full flying vehicle.

1 INTRODUCTION

High Aspect Ratio (HAR) wings are one of the best solutions to increase aircraft aerodynamic efficiency, reducing fuel consumption and carbon emissions. This can be achieved by increasing the wing span and using lighter materials. Nevertheless, as a consequence, the structures become more flexible. These slender, lighter wings come at the cost that they begin to exhibit higher levels of deformation and lower structural frequencies. Thus, HAR-wing aircraft show a coupling between flight dynamics and aeroelastic modes. Therefore, this coupling can no longer

be disregarded when analyzing the aircraft's flight dynamics because the rigid body approximation is no longer valid [1]. This coupling leads to changes in performance characteristics, flight dynamics, handling qualities, and aeroelastic stability with respect to the conventional aspect ratio wing aircraft. Thus, this increase in flexibility also affects stability augmentation systems and autopilots [2–4].

Since the 60s there have been different attempts to integrate structural dynamics into the Flight Dynamics Models (FDM). Nowadays, this integration is mandatory to represent the dynamics of HAR airplanes properly. There are different formulation approaches to model this kind of vehicle. These models can be classified in function of their different levels of fidelity and complexity. One of the main drivers of this classification is the difference between linear and nonlinear formulations to describe the structure. Another differentiation comes from the aerodynamic modeling, where quasi-steady, unsteady strip theory, vortex and doublet lattice, and CFD formulations can be implemented. It is also possible to include other nonlinear phenomena such as stall effects or following forces. With the increase in computational power is becoming more and more common that each research center and university laboratory produces their software to represent HAR aircraft. Focussing on this first structural classification some of the nonlinear-based formulations codes and toolboxes are UM/NAST (The University of Michigan's Nonlinear Aeroelastic Simulation Toolbox), SHARPy (Imperial College), and Aeroflex (Aeronautical Institute of Technology-ITA), NBS-Nonlinear Beam Shape (University of Bristol), Modal Rotation Method Formulation (Technion) [5–9].

A second class of software/toolbox classification has focused on modal superposition to describe the dynamics of the structure. This principle was proposed by Waszak and Schmidt (1988) [10]. These formulations are based on a set of nonlinear Equations of Motion (EoM) based on the small deformation assumption. Lagrange's equations and the principle of virtual work were used to generate the EoM. The EoM describe the structural movement relative to a "mean axes" body reference frame. This formulation allows the use of the free-free vibration modes of a normal modes analysis to fulfill the problem constraints automatically. Different programs and toolboxes make use of this formulation for example VarLoads (DLR), Loads Kernel (DLR), ModSiG (TU-Berlin), ITA-STAR (Aeronautical Institute of Technology-ITA), G-Flights (TU-Hamburg) [11–15].

To validate these models, it is necessary to perform aeroelastic experiments in wind tunnel facilities and flight test experiments. So far the flight test experiments are limited to flying demonstrators. Toolboxes like UM/NAST and ITA-STAR have been involved in different validation campaigns with the X-HALE and ITA X-HALE [16], [13]. This is a flying demonstrator with a High Altitude Long Endurance (HALE) aircraft configuration, allowing multiple levels of flexibility. Multiple pods along the wing distribute the instruments and payload. It allows for gathering coupled data on the structural dynamics and the rigid body. The aircraft has strain gauges and IMUs to collect the structural dynamics coupled with a central IMU/INS to collect the CG motion dynamics. It permits performing inflight systems identification experiments and control for high aspect ratio wings. Another platform used to study complex aeroelastic phenomena is the FLEXOP/T-Flex aircraft [17]. This aircraft has a motor-glider configuration and was designed to help develop control methodologies for active flutter suppression and passive load alleviation. It is also used for in-flight system identification and model tuning [18], [19].

Other aeroelastic experiments have been built in the form of wind tunnel experiments to generate data for model validation and control of very-flexible/flexible HAR wings. The Pazy wing

is a very flexible wing model designed to study nonlinear aeroelastic phenomena. It was the result of a collaborative effort within the Third Aeroelastic Prediction Workshop and part of the Large Deflection Working Group (LDWG) and was designed and built by Technion. This unswept wing is capable of presenting elastic deformations up to 50% with respect to the span and has been part of different works in model validation, flutter prediction, and aeroelastic identification [20], [21]. The Pitch-Free Flexible High Aspect Ratio Aircraft Model is a wind tunnel model with a generic airliner configuration built at the University of Bristol. The 1.72 m span model is capable of carrying wings with different levels of flexibility 5% and 15% vertical wingtip deflection. It was installed on a 3DOF gimbal that constrains yaw and roll and allows only for pitch-free motion. The data from this wind tunnel test allowed to validate a model based on low-order geometrically exact nonlinear elements coupled with different aerodynamic formulations [8]. The EASE wing is a wind tunnel aeroelastic experiment that is allowed to have free pitching motion about CG, it was designed and built at the University of Michigan [22]. This half-airplane configuration has a stiff fuselage/tail assembly and was designed to carry a wing with a geometrically nonlinear behavior. The 1.5 m span wing uses IMUs (accelerometers and gyroscopes) for aeroelastic control and has load cells, strain gauges, and fiber optic systems to measure the behavior of the structure. The authors implemented an MPC controller to reduce the bending moment on the wing root. The Politecnico di Milano and the GLAMOUR consortium developed a wind tunnel model of a 1:6 scaled-down transport aircraft configuration. The half-aircraft model was connected to the floor and installed to a support that offered a free-free motion in plunge and pitch. This system permits trimming the aircraft in different flight conditions. The model was used to test different gust alleviation and flexible aircraft model strategies [23]. NASA and Boeing are also interested in developing control techniques to improve the performance and safety of HAR flexible aircraft. They adapted the Common Research Model (CRM) to carry a 13.5 aspect ratio wing. The CRM wing uses trailing edge mini flaps to regulate and alleviate loads in the structure. A wind tunnel model of the half airplane was built to be tested on the NASA Langley Research Center Transonic Dynamics Tunnel. The test plan for this wing was divided into two phases, phase 1 consists of the validation of the open-loop characterization of the wing. Phase 2 aims to test controllers for drag optimization, maneuver and gust load alleviation, and active flutter suppression [24].

To contribute to this line of research, the Chair of Flight Mechanics, Flight Control, and Aeroelasticity (FMRA) from the TU-Berlin and the Institute of Aeroelasticity of the DLR (DLR-AE) have engaged in the design and construction of an aeroelastic flying demonstrator capable of representing the dynamics of HAR aircraft. TU-Flex is a flight demonstrator with a transport aircraft configuration and high aspect ratio wings [25–27]. This platform allows for gathering coupled experimental data on the flight and structural dynamics of the aircraft. With a design that permits easy wing exchange, the aircraft can be tested with different wing sets with variable (increasing) levels of flexibility. The first version of the aircraft can carry a Flexible Wing (FW) set with wingtip deflections around 10% of the wing semi-span. Additionally, it can accommodate a Very Flexible Wing (VFW) with wingtip deflections of up to 20%. The TU-Flex is presented in Fig. 1. The aircraft is instrumented with eleven IMUs in the wings, tails, and fuselage, it also has three strain gauges measuring points in the wing. The flight dynamics are monitored via IMU with a magnetometer and GPS in the CG. The aircraft also carries a 5-hole pitot probe to measure velocity, angle of attack, and sideslip angle. The demonstrator is electrically powered by batteries and two electric ducted fans provide the propulsion. Since HAR flexible aircraft dynamics are complex, the validation process requires a low to high-complexity approach. Therefore, the validation process was organized to start with the structural and aeroe-

lastic models. The resulting tuned models will be used to design the flight testing campaign before the full flight dynamics model can be validated.

Figure 1: TU-Flex and systems

The objective of the present work is to show the results of a static, GVT, and wind tunnel test campaign to validate a HAR flexible wing model. These experiments were applied to the TU-Flex FW to gather the data necessary to validate the structural and aeroelastic models. One of the design requirements of the aircraft was that the half wing could enter one of the available wind tunnels for the FMRA and the DLR-AE. The selected wind tunnel for this research was the Crosswind Simulation Facility (SWG) at the DLR-AE in Göttingen. The test section is suitable for performing static and dynamic tests. The SWG facilities are shown in Fig. 2. This experimental campaign is part of the validation process of the TU-Flex demonstrator model. This bottom-to-top validation approach allows us to isolate different physical phenomena with the overall goal of validating the model of a HAR flying demonstrator with very flexible wings.

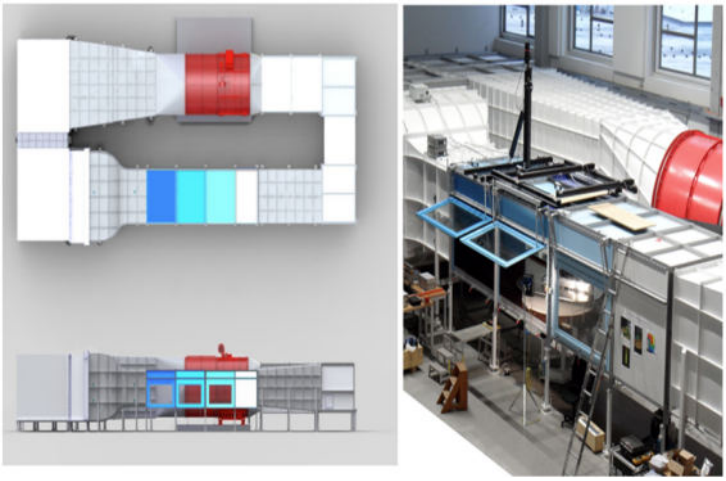

Figure 2: Crosswind Simulation Facility (SWG) at the DLR-AE [28]

The remaining sections of the paper are organized as follows. Section 2 presents the description of the TU-Flex´s FW and its systems, it also describes the different models used to design the experiment. The third section describes the different tests and how they were designed. The fourth section summarizes some important cases evaluated during the test campaign. It shows static, dynamic, and aeroelastic data with a first comparison with our structural and aeroelastic

models. Finally, some conclusions and future works are presented in the fifth section.

2 TU-FLEX´S FLEXIBLE WING

This section describes the wing geometry and structure as well as the systems and sensors installed in the wing and used for the wind tunnel experiment and the aeroelastic model validation. This wing has more strain gauge measurement points than the wing installed on the aircraft. The IMUs and servos are the same.

2.1 Wing Geometry and Sensors

The TU-Flex FW has two spars at 20% and 70% chordwise, as presented in Fig. 3. The skin of the wing is the main load-carrying structure. This wing is the result of an aeroelastic tailoring optimization process. The wing design requirements targets were maximum deflection while minimizing the weight and reducing the first bending mode frequency to increase its coupling with the short-period mode in the free-flying aircraft. The wing has three structural design fields, in each of these fields the skin changes thickness. It starts with a greater thickness in the root with six plies of glass fiber, then four in the middle, and ends with only two plies in the tip of the wing. The detailed description of the design process of the wing is presented in [26]. The root of the wing is integrated with the fuselage, therefore it has the geometry change in the root. A joiner was designed and built in-house to adapt the wing root to the balance system of the wind tunnel. The joiner is made of five pieces of aluminum, it has the same fixation points as the aircraft fuselage. This was done to simulate as closely as possible the same boundary conditions of the wing in the airplane at the same time that it was suitable for the wind tunnel connection. The TU-Flex wing has an aspect ratio of 16 and the length of the half wing is 1.8 m span. The chord in the root is 0.3 m and 0.15 m in the tip. The thickness of the airfoil is enough to store all sensors and actuators inside the aircraft.

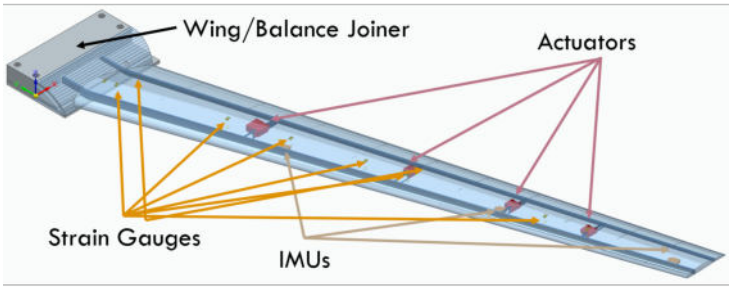

Figure 3: TU-Flex´s Wing with wind tunnel joiner

The wind tunnel wing has eight strain gauge points along the wing, six to gather bending deformations and two to gather in-plane motion. This data is gathered via an analog connection and then sent to the wing Data Acquisition System (DAS). The main processor of the wing is an STM-32 Discovery 4, a high-performance microcontroller capable of handling, SPI, CAN-BUS, PWM, UART, analog and PWM signals and communications protocols. The wing also has three IMUs evenly distributed along the span, they are capable of gathering linear accelerations, and angular rates, and estimating their Euler angles. This IMUs are connected via SPI to the DAS. The wing has four control surfaces: a flap and three ailerons. The flap is operated with a Volz servo DA20 and activated via a PWM signal. The three ailerons were designed for roll and structural regulation control. They are activated by three Volz servos DA15 via CANBUS connection. All servos are capable of measuring the deflection angle and sending it to the DAS. The DAS gathers all data at 100 Hz and allows the input of a synchronization signal from the wind tunnel balance and flow velocity measurement system. The wing systems distribution and

Table 1: General properties of the TU-Flex FW.

Property	TU-Flex FW
Span	1.8 m
Chord (root)	0.30 m
Chord (tip)	0.15 m
Taper ratio	0.5
Aspect ratio	16 (full wing)
Sweep	20 deg
Wing area	0.405 m^2
Mean chord	0.225 m
Airfoil max thickness	11.1 %
Wing mass	2.2 Kg

communication protocol description is presented in Fig. 4. Table 1 presents the main properties of the TU-Flex FW.

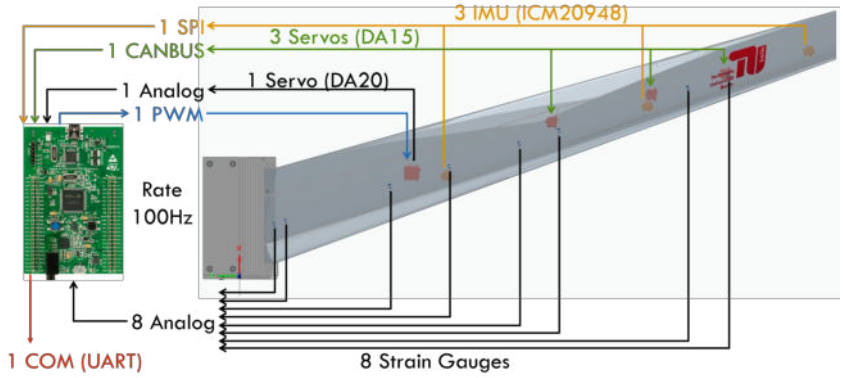

Figure 4: TU-Flex´s Wing sensors and acquisition system connection

A fairing was built to reduce the flow disruption coming from the wing/joiner assembly. This fairing was fixed to the aluminum joiner and was designed to minimize contact with the wing structure. The wing-joiner-fairing assembly is presented in Fig. 5. The dotted points on the upper skin were painted to allow for an optical measurement system to capture the wing motion. This system has not been available for this test campaign.

Figure 5: TU-Flex´s Wing installed in the wind tunnel

2.2 Wing Models

Multiple models were created to assist the design process of the wing and the wind tunnel experiments. An iteration process was applied to define the different test points in the wing

tunnel. The wind tunnel boundary condition allows the users to place the wing in positions that can be outside the flight/loads envelope. Therefore, it is mandatory to evaluate the safety of each of the test points. Three numerical frameworks were used to design the wind tunnel experiments: NASTRAN, Loads Kernel, and ModSiG.

2.2.1 NASTRAN

NASTRAN was used inside a framework developed to design the wing. This framework uses ModGen to create the geometry of the wing and size all structural elements [26, 27]. ModGen is a program aimed at generating structural FE and aerodynamic models of wing- and fuselage-like aircraft components compatible with MSC.NASTRAN, suited for GFEM/Dynamic and aeroelastic analyses [29, 30]. NASTRAN SOL-200 was used to size the structural elements of the model. The TU-Flex´s wing Finite Element Model (FEM) is mostly made of thin-walled composite laminates. Therefore, shell elements (CQUAD4 and CQUAD3) were used to define the skin and the spars of the wing. All the wing is made of the same glass fiber with different orientations to meet the material and performance requirements. The core of the wing is made of foam and it is modeled with solid elements (CHEXA and CPENTA). The NASTRAN aerodynamic model uses a panel mesh for the implementation of the DLM. The wing is represented as a flat panel using CAERO1 and AESURF cards. The camber and twist of the airfoil were also added with additional terms that allowed to include this correction. The servos and sensor weights are also present in the model as point masses elements. The optimization results output provides the material properties of the wing per design field. Each of the three design fields has a different material property. PyTLO was then used to turn these properties into an actual stack-up sequence that can be manufactured. The boundary conditions for this stack-up sequence were +-45 degrees plies of glass fiber [31].

2.2.2 Loads Kernel-DLR

Loads Kernel is a loads analysis software that couples aerodynamics and structural models to perform aerodynamic analyses of aircraft [12,32,33]. This program allows for the evaluation of different maneuvers, trim conditions, and load cases. It also includes features for unsteady gust loads and dynamic landing loads. The program is capable of defining multiple monitoring stations to calculate section loads for specific structural components. Additionally, the software is able to use the mass and stiffness matrices to perform modal analysis, because the deformation of the structure under aerodynamic forces is calculated via a modal superposition approach. This allows the user to generate combined structural and aerodynamic models including the masses inside the aircraft. In the aero-structural coupling, the structural and the aerodynamic nodes are associated using a nearest-neighbor algorithm. In this research, the program was modified to allow for fixed angle of attack (AoA) requirements. With this new boundary condition, the users were able to evaluate the response and loads on the wing tunnel model for static loads and dynamic maneuvers consisting in variations of angles of attack in the root of the wing.

2.2.3 ModSiG-FMRA Model

ModSiG-FMRA is a low-order framework for modeling, analyzing, and simulating very flexible/flexible wings and free-flying aircraft developed at the FMRA [14]. This program is based on nonlinear flight mechanics, and modal superposition for the structure, allowing the incorporation of quasi-steady and/or unsteady aerodynamics, including following forces and/or stall effects depending on the level of complexity selected by the user. The program performs numerical linearization, aircraft visualization, real-time simulation, and control evaluation [34]. The ModSiG-FMRA framework was used to assist the design process of the wind tunnel tests for

the TU-Flex FW. The model consists of a half-span wing model based on modal superposition, selecting incremental unsteady aerodynamics due to elastic deformations, using strip theory and indicial functions [14, 35]. It is possible to insert wind perturbations and to enforce rotations of specific nodes of the structure. The wing root AoA is set as an input to the model, allowing the implementation of static or variable rotations of the half-span wing. The framework uses the f06 output from a NASTRAN SOL103 to describe the structure via modal superposition. The aerodynamic distributions of the wing and control surfaces are calculated via VLM. The lift distribution is then added to the model via splines.

Figure 6 shows a comparison between NASTRAN, Loads Kernel, and ModSiG aeroelastic models. The plot shows the behavior of the wing for an AoA sweep from -6 to 6 degrees at 30 m/s. It is possible to see how the vertical displacement of the wing changes as a function of the AoA and the good agreement between models and formulations. For this case, the wing tip vertical excursion goes from -0.00198 m (-0.11%) to 0.1927 m (10.71 % half span). Both ModSiG and Loads Kernels models produce a slight overestimation of vertical deflection compared to NASTRAN. The highest error in Loads Kernel compared to NASTRAN occurs in the 4 degree AoA case with the deflection being overestimated by 4.5%. The highest error in ModSiG compared to NASTRAN occurs in the 5 degree AoA case with the deflection being overestimated by 1.45%. These models were used to design the maneuvers and test cases for the static and wind tunnel tests. All test cases, load conditions, and safety requirements were evaluated in these models before approval for the experimental test.

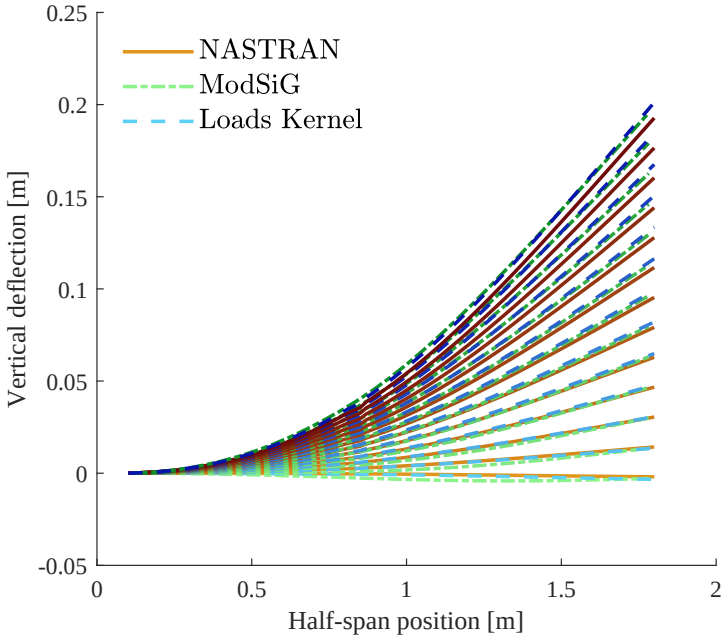

Figure 6: Comparison between aeroelastic models for an AoA sweep from -6 to 6 degrees (darker colors correspond to a higher angle of attack)

3 STATIC, GROUND VIBRATION, AND WIND TUNNEL TESTS DESCRIPTION

The test campaign for the structural, dynamics, and aeroelastic validation of the wing models was organized into three phases: static, ground vibration testing, and a wind tunnel test. Each of these processes was assisted by the models previously mentioned. An outcome of this iterative process gave an idea of which tests were inside the load envelope and could generate valuable data for model validation. The limits of the formulation and the strains were used to define the

different Load Cases (LCs). The acceptance of these LCs depended on two boundary conditions. The first one, no load case should generate a vertical wing tip deflection above 12% of the half span of the wing because this point was defined as a limit for the system's linearity. The second boundary condition had a higher limit of 6000 $\mu\varepsilon$ deformation on the skin wing. This value was set as the maximum allowable strain for the structure with a safety margin of 1.5. All evaluated load conditions respected these limits and were simulated before the experiments. The whole structural and aeroelastic test campaign workflow is shown in Fig. 7. These tests will be described in more detail in the following subsections.

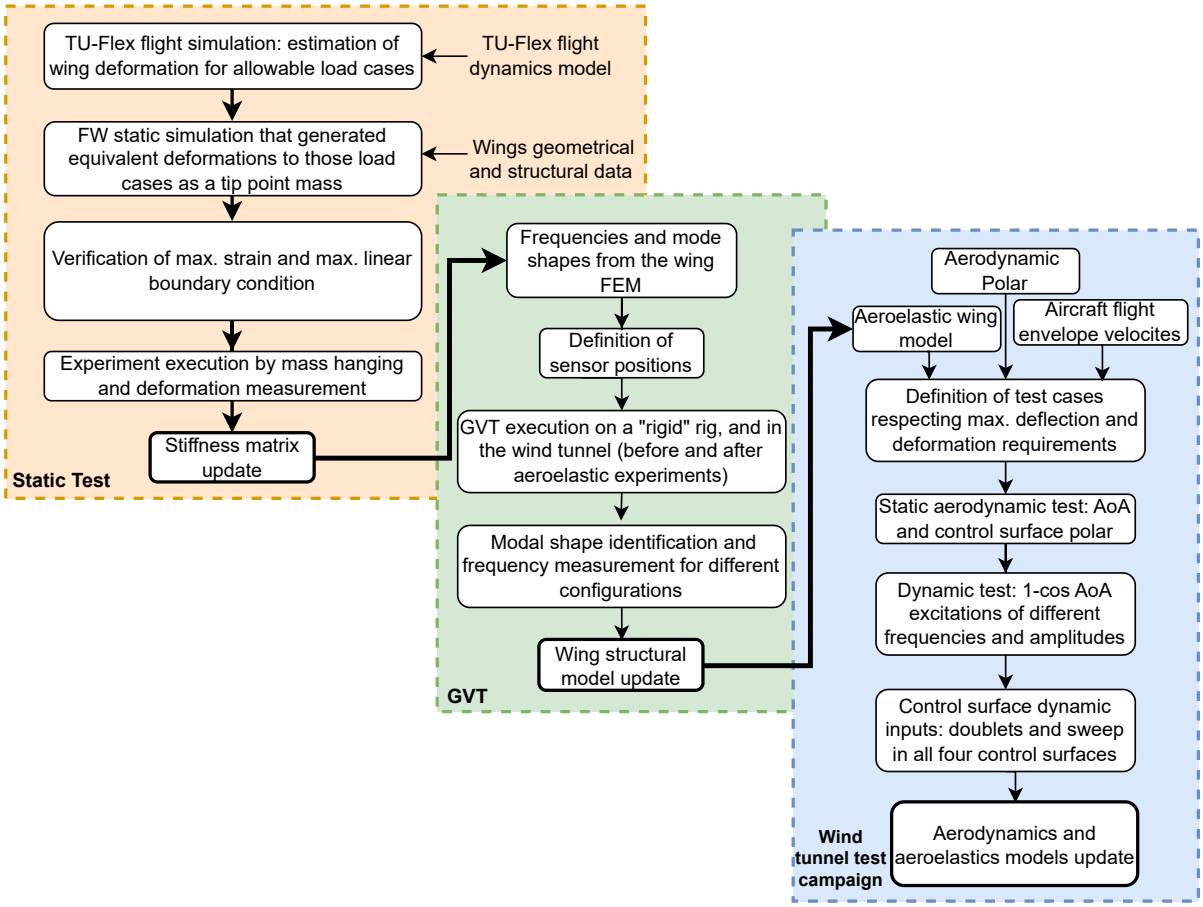

Figure 7: Structural and aeroelastic test campaign description

3.1 Static Test

The objective of the static test is to generate data to tune the stiffness matrix of the structural model. In this way, all coupling with mass, inertia, and aerodynamics can be eliminated and a clear estimation of the stiffness of the built wing can be extracted.

The wing was installed in the wind tunnel joiner to prepare the experimental setup. Then, the whole assembly was clamped to a workstation with a high mass and stiffness. A rig was built to install a laser and a visual measurement system. Due to the high levels of deformation, the laser system was only available for the first two load cases. The rest of the measurement points were directly measured with a ruler. Fourteen Load Cases (LC) were considered for the static test:

$$LC = [-1.5g, -1g, -0.75g, -0.5g, -0.25g, \\ 0.25g, 0.5g, 0.75g, 1g, 1.25g, 1.5g, 1.75g, 2g, 2.5g] \tag{1}$$

These load cases were selected using the full-flying TU-Flex model using Loads Kernel and ModSiG. The aircraft was loaded until these LCs were achieved and then, the respective deformations and vertical wingtip deflections were extracted. Later, a concentrated force was applied at the tip of the wing and simulated as a static problem in NASTRAN. The magnitude of these forces was tuned to match the level of deflection observed on all LCs on the flying aircraft. Thus, the static test was designed so that a single mass applied to the wing tip could cause these deflections. All these LCs were evaluated in NASTRAN using SOL101 before the experiments. For numerical validation, the same static simulations were performed in Loads Kernel and ModSiG for confirmation.

3.2 GVT

The Ground Vibration Test (GVT) was designed to measure the vibration modes frequencies and modes shapes of the wing. This data will be used to tune the structural model of the wing. The test cases were designed to measure the structural dynamics of the different structural components and to evaluate the influence of the actuators and electric systems on the dynamics of the wing.

To perform this test, the FMRA counts with a Siemens SCADAS acquisition system, 15 uniaxial accelerometers, an excitation hammer, and the Simcenter Teslab software for modal analysis. Previously, the FEM was used to identify the frequencies and shapes up to 160 Hz. Four sensor configurations were proposed to acquire the dynamic response of the wing. Configuration 1 was designed to gather the dynamics of the main structural components of the wing. The accelerometers (ACCLRM) were evenly distributed on top of the front and rear spars of the wing. Configuration 2 was designed to verify the stiffness of the servo's linkage to the control surfaces. The ACCLRMs were placed on the top of the front spar and in the same line as the position of the linkage. A second line of ACCLRMs was placed on the rear spar to facilitate the interpretation of the results. Then, a last row of ACCLRMs was installed on the tip of all four control surfaces. Configuration 3 was created to replicate the wing sensor distribution. The ACCLRMs were installed on top of the strain gauges and IMUs installed in the wing. This configuration is to verify the quality of the modes and frequencies that could be estimated by the wing sensors. Finally, Configuration 4 was designed to measure the in-plane modes of the wing. The FEM showed two in-plane modes present within the first 150 Hz. This setup used five 3d printed adapters to place the ACCLRMs in the in-plane orientation and allow the measurement. Four hit points were used to excite the system during the GVT. Two in the center and trailing edge of the wing tip, one on the front of the wingtips leading edge in the in-plane orientation. A four-hit point was used in the wing center to excite higher-frequency bending modes. Figure 8 shows the ACCLRMs distribution for all four configurations and the hit points.

The wing GVT, for Configurations 1 to 4, was first performed in a high-density high-stiffness rig as shown in Fig. 9. Then, the wing and joiner assembly was installed in the wind tunnel. A second GVT for Configurations 1 and 4 was performed there, to verify if there were other modes coming from the motor or the balance connection. After the wind tunnel campaign was completed, a third GVT on Configuration 1 was completed. Figure 10 shows the GVT set up

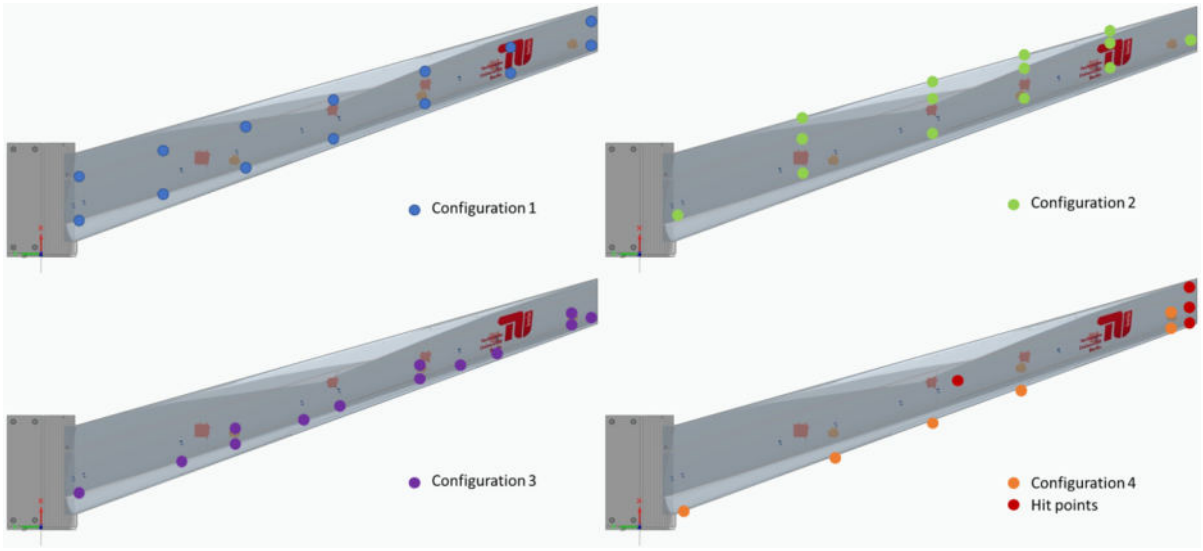

Figure 8: TU-Flex´s wing with wind tunnel joiner.The blue, green, purple, and orange dots show the ACCLRMs' positions for each configuration, while the red dots show the hit points' positions used for all configurations

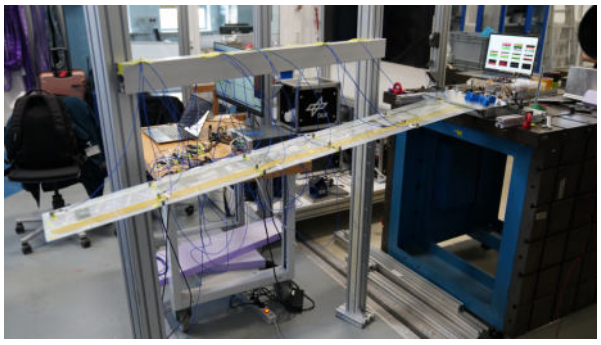

Figure 9: GVT set up in the "rigid" rig

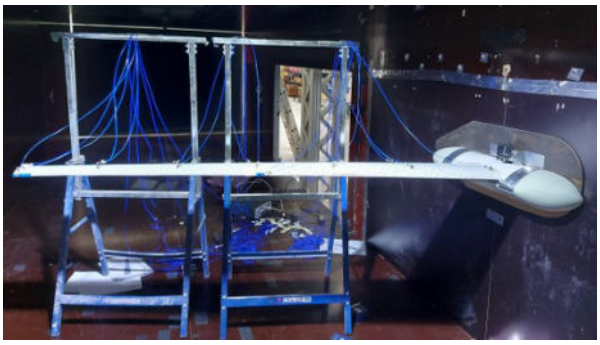

Figure 10: GVT set up in the wind tunnel test

inside the wind tunnel. The objective of this third test was to verify if there were any changes in the dynamic behavior of the structure due to any residual plastic deformation due to the load of the test. All tests were executed three times to increase the reliability of the acquired data. Finally, all tests were performed with the electric system on and off to verify the influence of the actuator stiffness in the dynamics of the wing. This also allowed to gathering of data for systems identification using the wing's internal sensors.

3.3 Wind Tunnel Test

The test section of the Crosswind Simulation Facility wind tunnel is 2.4 m x 1.6 m x 9 m (W x H x L). The wind tunnel can stabilize the airflow from 12 m/s to 65 m/s [36]. The wind tunnel allows the change of one of the test section walls to meet all geometry constraints of the models. A service wall was built for the TU-Flex FW with the dimensions of the joiner and with enough space for the balance to be connected and to leave room for the cables coming out of the wing. Figure 11 shows the wing installed on the SWG with a fairing to smooth the interaction between the root section of the wing and the airflow. A blocking plate was also built to seal the access wall.

The objective of the wind tunnel test is to generate data for the aerodynamics (considering the deformation of the wing) and the aeroelastic model validation. The wind tunnel balance was

capable of recording forces and moments acting on the root of the wing at the same time the electric system of the wing was activated and measuring all available accelerations, angular rates, and loads along the wing. The balance uses a piezoelectric system developed by the DLR-Institute of Aeroelasticity. It consists of four 3-component force measuring elements. Each force-measuring element has one quartz crystal pair per coordinate axis. The electrical charges emitted by the crystals are proportional to the acting forces. In an amplifier, the charges are converted into electrical voltages. Then, they are digitized in an analog-digital converter and further processed in the measuring computer. This balance allows measuring vertical and horizontal forces, as well as, torsional and bending moments. A laser sensor was installed on the wind tunnel to measure the AoA by measuring the rotation of the wing joiner. The SWG-installed servo motor allowed fixing an AoA and inserting 1-cos dynamic inputs. The motor, balance, and AoA measurement system are shown in Fig. 12. The TU-Flex FW was evaluated at different speeds: $[18m/s, 22m/s, 30m/s, 34m/s, 40m/s]$. These speeds were selected based on the aircraft's flying envelope: the expected stall speed, minimum speed to fly, cruise speed, Carson speed, and max speed to test, respectively.

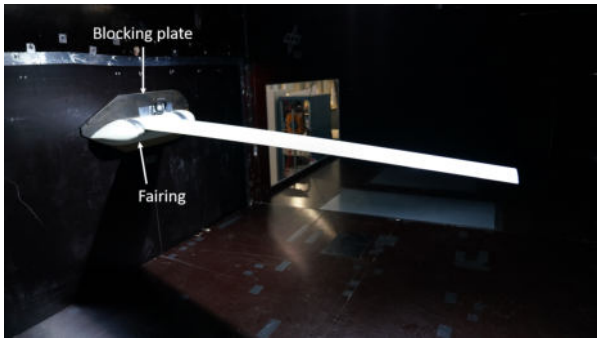

Figure 11: TU-Flex FW installed on the SWG

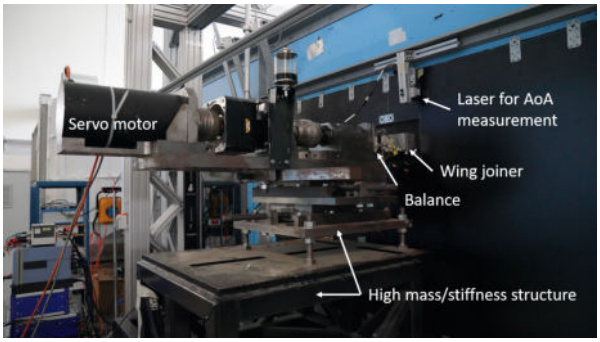

Figure 12: Motor with Balance in the SWG

The wind tunnel test was organized into three phases:

- Phase 1 consisted of static aerodynamic measurements. To validate the aerodynamic model, the wing was placed in different AoA until the aerodynamic polar was completed (from the negative stall AoA to the positive stall AoA). This phase consists of slow variations of AoA. Each time a new angle of attack was reached, the acquisition of the transient and the steady state was performed.
- Phase 2 was focused on dynamic variations of AoA. The dynamic maneuvers were 1-cos variations of the AoA in the root with different frequencies and amplitudes.
- Phase 3 was concentrated on control surface inputs. The idea was to record the response of the wing to steps, doublets, and frequency sweeps at different velocities. The first control surface test is a sequence of steps that are hold for 10 seconds. The doublets were actuated with different amplitudes. The Doublet is a 2 s maneuver going positive and then negative (1s on each side) and holds for 10s to stabilize the wing. The Sweep is a sinusoidal maneuver with variable frequency from 0 to 10 Hz within 30 s. After that, it is held at 0 degrees for 10 s. The flap and all three ailerons were used independently in this phase.

4 RESULTS

The results section is separated into three subsections: static, ground vibration, and wind tunnel tests.

4.1 Static Test

Figure 13 shows the static test setup. The upper left picture shows the wing under the gravity load. This was considered as the reference point of the test. The side view shows the reference line of the test. A hanging bar was adapted to the wind surface to hang the load masses. All LCs were applied and measured four times between the loading and unloading procedures. The maximum load case of 2.5 g is presented in the lower part of Fig. 13.

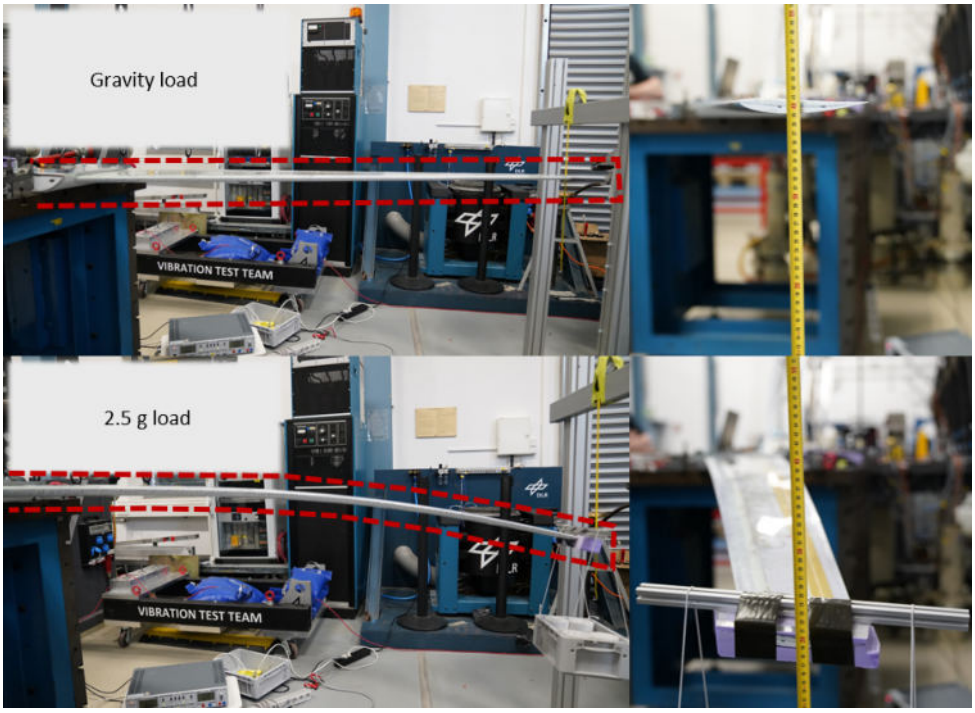

Figure 13: Unloaded and maximum load case deformation during the static test

Table 2 shows the summary of the static test. It presents the weights loaded on the wing tip that produced the equivalent deformation for the desired LC. The table also shows the average of the measurement in vertical wing tip displacement relative to the 0g LC and the percentage with respect to the half span. The corresponding vertical wing tip displacement calculated using the NASTRAN model is in the table's fifth column. A SOL 101 static analysis was used to produce this output. The last column shows the error between the model and measurements.

Figure 14 shows the vertical wing tip displacement as a function of the Load Case. It is possible to verify that the wing excursion goes from 11.69% (2.5 g) to -5.57% (-1.5 g). The total vertical wing tip excursion of the wing is 17.26 %. Error bars were added to the plot to show the dispersion of the measurements. The plot allows us to see the linear behavior of the wing between the -1 and 2.5 g LCs. The error between modeled and measured displacement is largest in the -1.5 g LC. Here the deformation is overestimated by 1.635% of the half-span. It is possible that for this LC the wing is already showing non-linear behavior in its deformation. The mean magnitude of the error between the model and measurement neglecting the -1.5 g case is 0.285% of the half-span.

Table 2: Static test measurements LC (load Case), W (Weight), TDA (measured Tip Displacement Average), MTD (Model Tip Displacement)

LC (g)	W (kg)	TDA [m]	TDA [% span]	MTD [% span]	error [% span]
-1.5	2.687	-0.1003	-5.57	-7.20	-1.635
-1	1.694	-0.0795	-4.42	-4.80	-0.386
-0.75	1.197	-0.0609	-3.38	-3.60	-0.219
-0.5	0.787	-0.0413	-2.29	-2.61	-0.317
-0.25	0.33	-0.0223	-1.24	-1.50	-0.268
0.25	0.33	0.0218	1.21	1.50	0.296
0.5	0.787	0.0426	2.37	2.61	0.241
0.75	1.197	0.0604	3.35	3.60	0.247
1	1.694	0.0821	4.56	4.80	0.240
1.25	2.687	0.1034	5.74	6.01	0.262
1.5	3.183	0.1235	6.86	7.20	0.344
1.75	3.684	0.1464	8.13	8.40	0.272
2	4.684	0.1683	9.35	9.62	0.269
2.5	5.684	0.2105	11.69	12.03	0.340

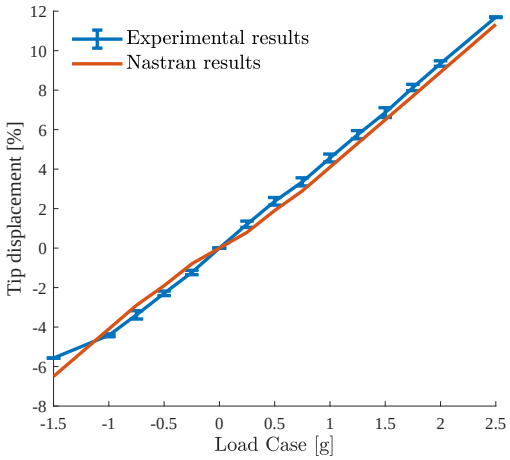

Figure 14: Numerical and experimental test comparison

4.2 GVT

The ground vibration testing of the wing was performed to identify the frequencies and shapes of the wing and to identify if there was any substantial change between the dynamics of the wing before and after the wind tunnel test. All four configurations were tested in the rigid rig (Fig. 9). Nevertheless, only Configuration 1 and a modified mix between Configuration 1 and 4 were tested in the wind tunnel. The results shown in Fig. 15 only include results from Configuration 1 in the rig and wind tunnel.

Figure 15 shows the measured frequencies of the TU-Flex FW in the GVT rig and installed in the wind tunnel motor. The target of the test was to identify the first eight wing modes. For the GVT done in the rig, it is possible to see the main eight peaks of the natural frequencies of the wing. The measurements of Configuration 4 were added to this curve to include the two in-plane modes. The first, second, and third bending, the first torsion, and the first and second in-plane have damping of around 1.2% on average. The fourth and fifth bending are more damped modes with 4.5% and 3.5% of damping, respectively. The most difficult mode to identify was the first torsion due to its small amplitude. It was normally overlooked due to the larger magnitude of the

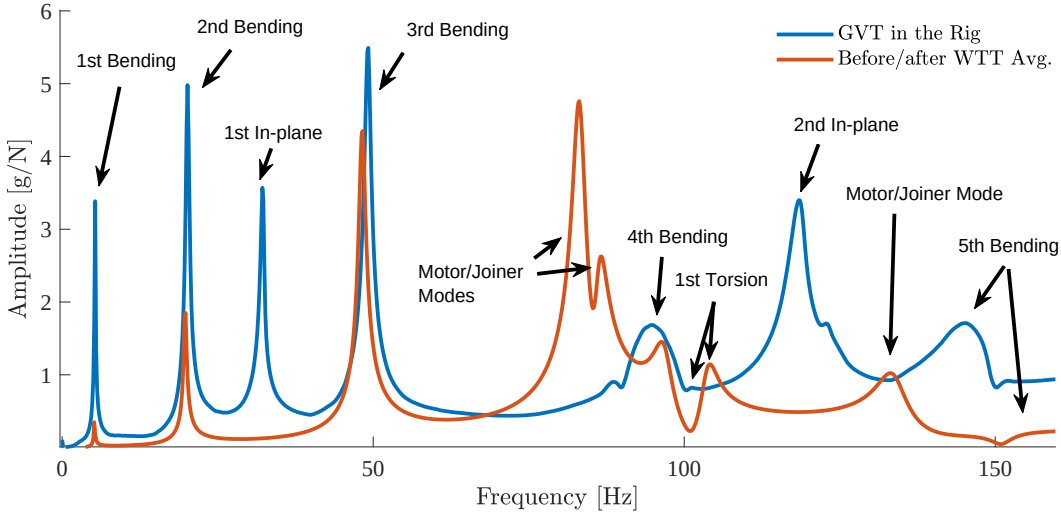

Figure 15: Measured frequencies

Table 3: Summary and comparison between measured and FEM modes on the GVT rig.

Summary of the modes	Average GVT [Hz]	FEM [Hz]	error %
1st bending	5.297	5.25	0.88
2nd bending	20,160	20.81	-3.12
1st In-plane	32.269	31.92	1.09
3rd bending	49,130	49.67	-1.08
4th bending	92.866	94.03	-1,23
1st Torsion	103.560	120.52	-14.07
2nd In-plane	122.681	125.30	-2.09
5th bending	149.18	151.63	1.64

fourth bending. However, once it was isolated using the Polymax toolbox in Simcenter, it was possible to identify the torsion. Table 3 shows a summary of the frequencies of the first eight modes of the wing. The average error between all mode frequencies neglecting the first torsion is -0.56%. The biggest error is the modeling representation of the torsional wing behavior. The torsion stiffness seems to be overestimated in the FEM, with a difference of 14 Hz with respect to the measured frequency.

To evaluate the influence of the wind tunnel motor/joiner section in the modes of the wings, GVTs were done before and after the wind tunnel tests. The orange line in Fig. 15 shows the average frequencies in the wind tunnel facility. It is possible to see that the motor/joiner installation influences the frequencies of the modes. The first, second, and third bending were reduced by 0.16, 0.47, and 0.93 Hz, respectively. At the same time, the fourth bending, first torsion, and fifth bending were increased by 3.54, 0.64, and 3.78 Hz, respectively. It is interesting to point out that three new modes are present in the wind tunnel assembly. These modes appeared at 83.1 Hz, 86.7, and 132.9 Hz. The shapes of the first two motor/joiner modes are presented in Fig.16. It is possible to see that there is no noticeable movement of the wing structure while there is a distinctive movement on the root of the wing on the right-hand side of the plot.

The GVT measurements were used to validate the dynamic wing model. The identified modal shapes and frequencies can be compared with the FEM shapes and frequencies to assess the level of confidence in the model. One way to compare measured and simulated modal shapes

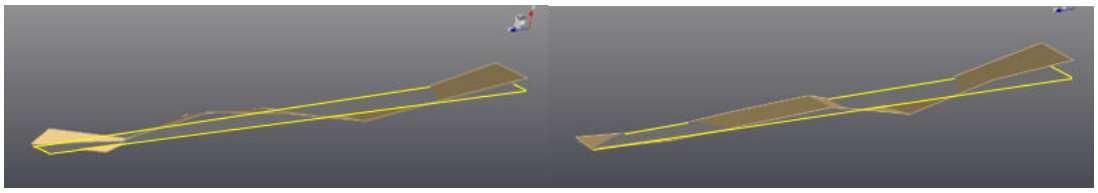

Figure 16: Motor/Joiner modes

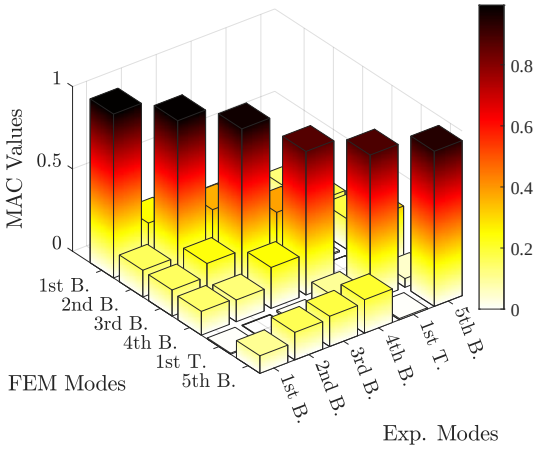

Figure 17: Bending and torsion modes MAC

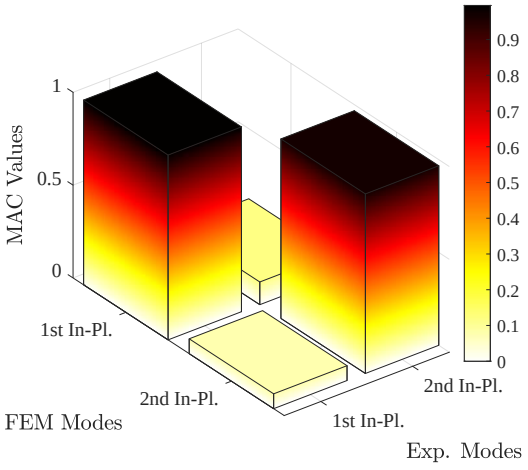

Figure 18: In-plane modes MAC

is the Modal Assurance Criterion (MAC) [37]. The MAC represents the degree of collinearity between two or more mode shapes. MAC can be employed to compare multiple mode shapes extracted from the FEM and estimated from the data collected from the corresponding structure. The MAC estimate is within the interval 0 and 1. If the mode shapes correspond to the same mode and are highly correlated, the resulting MAC estimate is close to 1. If the mode shapes are very different, the MAC value will be close to zero. The MAC for all bending modes and the first torsion comparing the mode shapes of the FEM and experimental measurements is presented in Fig. 17. It is possible to see a distinctive diagonal in the plot meaning that there is a high correlation between the FEM and the measurements. The first bending has a correlation of 0.995 in the MAC. The second, third, and fifth bending modes had a MAC of 0.989, 0.974, and 0.941, respectively. A smaller but still satisfactory correlation is present in the fourth bending and first torsion modes with a MAC of 0.871 and 0.884, respectively. The modes are not completely decoupled from each other. There is a certain similarity between the second and third bending and the third and the fourth. It is 0.36 and 0.38 on the MAC scale. The most isolated mode with respect to the rest is the first torsion with a maximum correlation with the fourth bending of 0.10 on the MAC scale. The MAC was also applied to the measurements of Configuration 4. The in-plane modes MAC is shown in Fig. 18. Another clear diagonal is observed in this case with a correlation of 0.995 and 0.967 for the two in-plane modes.

To further evaluate the similarity between the model and experiment the mode shapes were investigated. The estimated modes via Simcenter and the FEM modes are plotted side by side in Fig. 19. The modal shapes resulting from Configuration 1 have a better resolution than the modal shapes resulting from Configuration 4. The modal shape of Configuration 1 can show the moving surface of the wing skin in bending and torsion, whereas Configuration 4 measurements only describe a line in the in-plane. However, all animations are able to capture the modal shapes of the wing. Based on this correlation, it is possible to affirm that the FEM

modes shapes show a high level of similarity compared to the built wing.

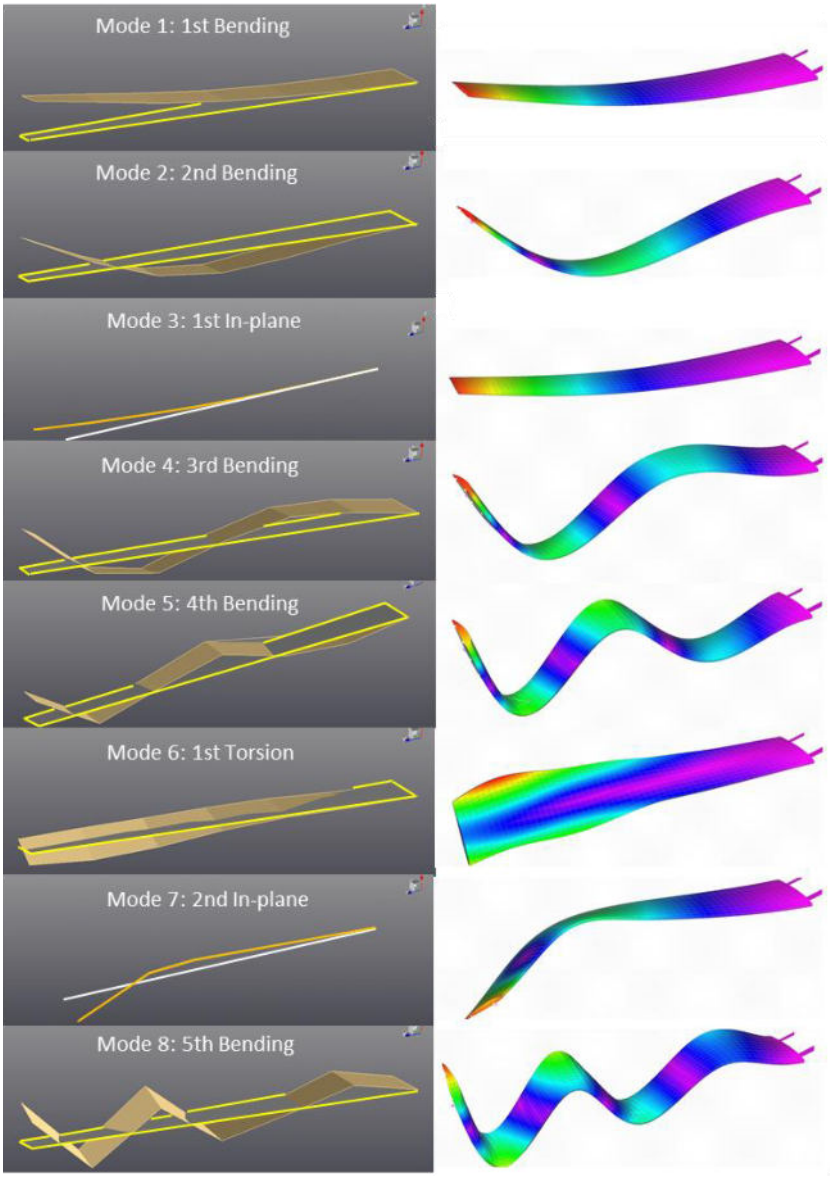

Figure 19: Comparison between the identified wing mode shapes and the FEM

4.3 Wind Tunnel Test

This subsection presents a preliminary post-processing analysis of the wind tunnel experiment data. During the test, it was possible to record the vertical and horizontal forces and the bending and torsion moments at the joiner/root section of the wing by the balance. The angle of attack of the joiner was also available in the joiner section. The wing was able to record all outputs: the eight strain gauges and the three IMUs, as well as the angles and commands of the control surfaces. All data was stored at 100 Hz and was available for real-time monitoring and control.

During the wind tunnel campaign, 385 test cases were performed. All these test cases fulfill the two safety boundary conditions for vertical wing tip deflection and maximum local deformation. Table 4 shows the number of test cases per velocity. The number of cases was reduced as the speed increased to respect the safety limits. Figure 20 top shows the rear and side views of the wing without wind load. The bottom pictures show the rear and side views of the wing for the maximum load case applied in the wind tunnel. This level of deformation corresponds to 40 m/s

Table 4: TC per velocity.

Velocity [m/s]	18	22	30	34	40	Total
TC amount	121	101	72	55	36	385

and 4 deg in AoA. The 5 white lines on the right wind tunnel wall correspond to -8%, -5%, 0%, 12%, and 16% of vertical wing tip deflection. They were installed to have a visual indication of the linear and nonlinear limits of vertical deflection of the wing in the wind tunnel.

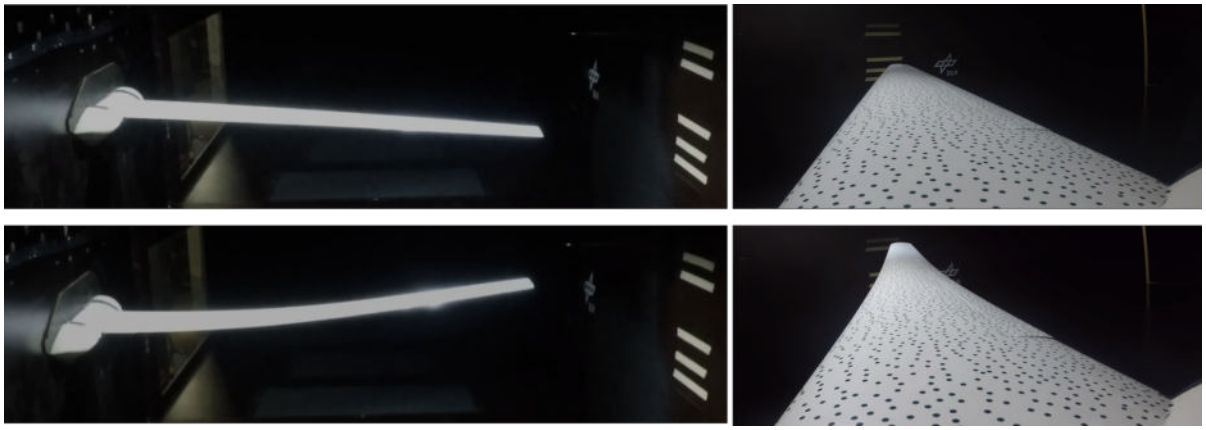

Figure 20: Unloaded and maximum load case deformation of the wing rear and side view

This paper presents three Test Cases (TC) to show the quality of the acquired data and the current state of the aeroelastic models. TC-1 and TC-2 were doublets control input maneuvers. The initial velocity for TC-1 was 30 m/s and 34 m/s for TC-2. The starting AoA for both cases was 1 deg. The doublet command for TC-1 was ± 5 deg on the external aileron, each excursion had a duration of 1 s. The TC-2 doublet command was also on the outermost aileron with an amplitude of ± 15 deg 1 s per side. TC-3 consists of an AoA variation using a 1-cos input. The initial velocity was 30 m/s and the initial AoA was 1 deg. The frequency maneuver was 4 Hz to have a safety margin of 20 % before reaching the first bending. The amplitude of the TC-3 was 4 deg, therefore the maximum AoA excursion reached 5 deg.

Figures 21 to 23 show the comparison between the untuned aeroelastic models used to design the maneuvers (also used in the preliminary design and analysis of the wing) and the data collected in the wind tunnel. Fig. 21 shows the vertical force, and the wing root bending moment, both normalized to their respective trim values and the vertical acceleration at the wingtip for the TC-1 case. Both models capture the trend of the maneuver satisfactorily. A positive aileron deflection causes all presented outputs to rise followed by the respective reduction and regulation once the doublet is completed. There is a 0.05 s delay between the actuator signal command and the actuator response. It is important to point out that, the models do not include the actuator dynamics. This can be noticed due to the time lag between the response of the numerical models and the experimental response. In this case, it is also possible to observe that, ModSiG has a 5 % lift increase overestimation with respect to Loads Kernel. There are also higher frequency responses present in the Loads Kernel dynamics. Nevertheless, they are damped out and both models can return to their initial condition. It is noticeable that ModSiG, while matching the dynamic behavior, significantly overestimates the magnitude of the vertical acceleration at the wingtip.

Fig. 22 shows the vertical force, root bending moment, and vertical acceleration for TC-2. The

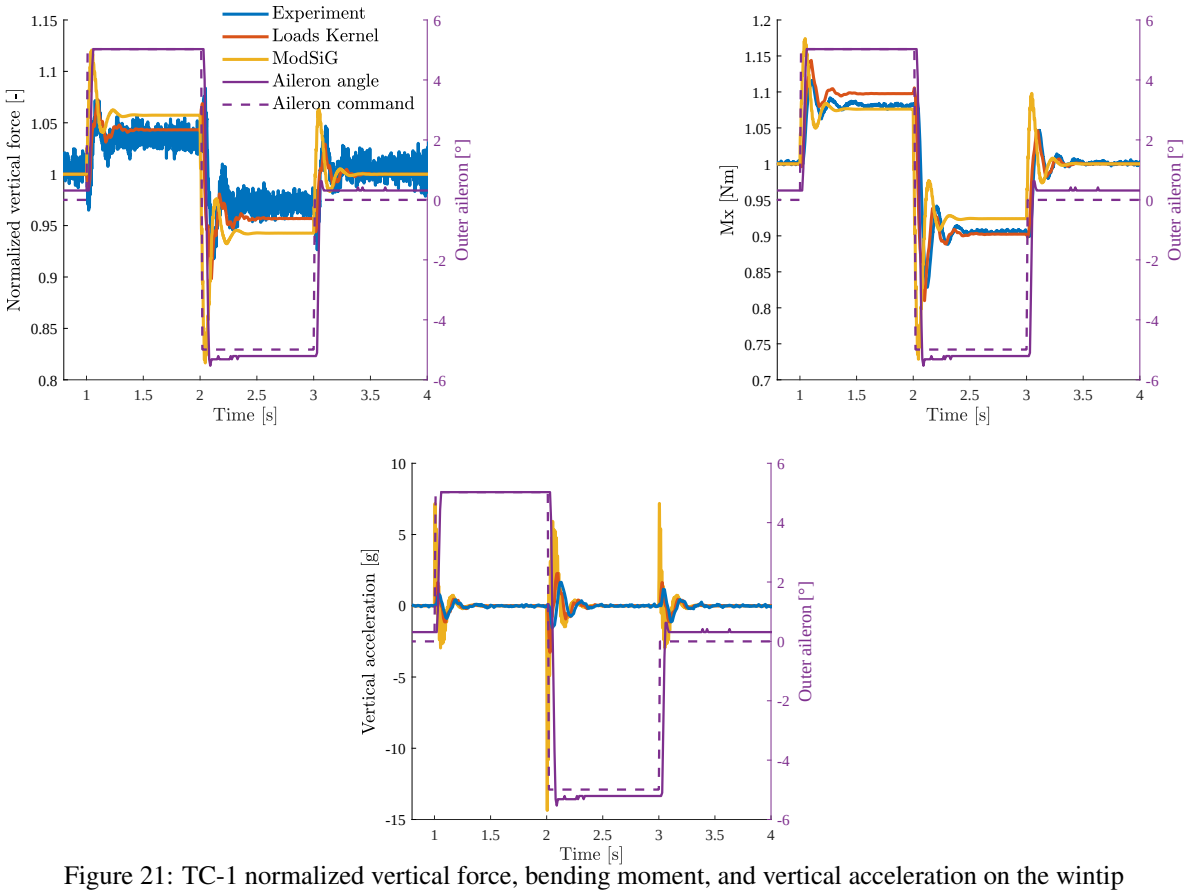

Figure 21: TC-1 normalized vertical force, bending moment, and vertical acceleration on the wintip

overall behavior is similar to TC-1. The amplitudes of the vertical force and bending moment are higher than in TC-1. Both models again are able to follow the trend of the maneuver. The delay between the actuator signal and response in the loads visibly increases compared to TC-1. This results in the peaks of the loads being offset between models and experiments by up to 0.1s. Loads Kernel now overestimates the amplitudes in the vertical force and bending moment, while ModSiG underestimates them. Both models overestimate the vertical acceleration during the aileron deflections. Loads Kernel again displays a higher frequency response during the maneuver. This type of maneuver will support the tuning process not only of the aeroelastic model but also of the control derivatives of the aileron to properly characterize the influence of the control surface in the wings dynamics.

Fig. 23 shows the normalized vertical force, root bending moment, and vertical acceleration for TC-3. Both models capture the overall behavior of the maneuver, with the vertical force and bending moment increasing with increasing AoA, then decreasing again and showing a small undershoot. Both models overestimate the loads during the maneuver. The response of the loads is delayed, with the highest loads in the experiment occurring 0.014s after the peak in AoA change. Both ModSiG and Loads Kernel also show a delay in the response of the loads. ModSiG's delay is 0.013s, Loads Kernel's delay is 0.032s.

Both models follow the overall behavior of the acceleration of the wingtip during the maneuver. In this case, the magnitudes between models and experiments are quite similar but with a phase delay. The peaks of the accelerations are out of phase by up to 0.06s. This could be caused by the lag in the measurement of the IMU as well as unidentified dynamics of the sensor which are not yet included in the models. As in the loads, the experiment shows a higher frequency

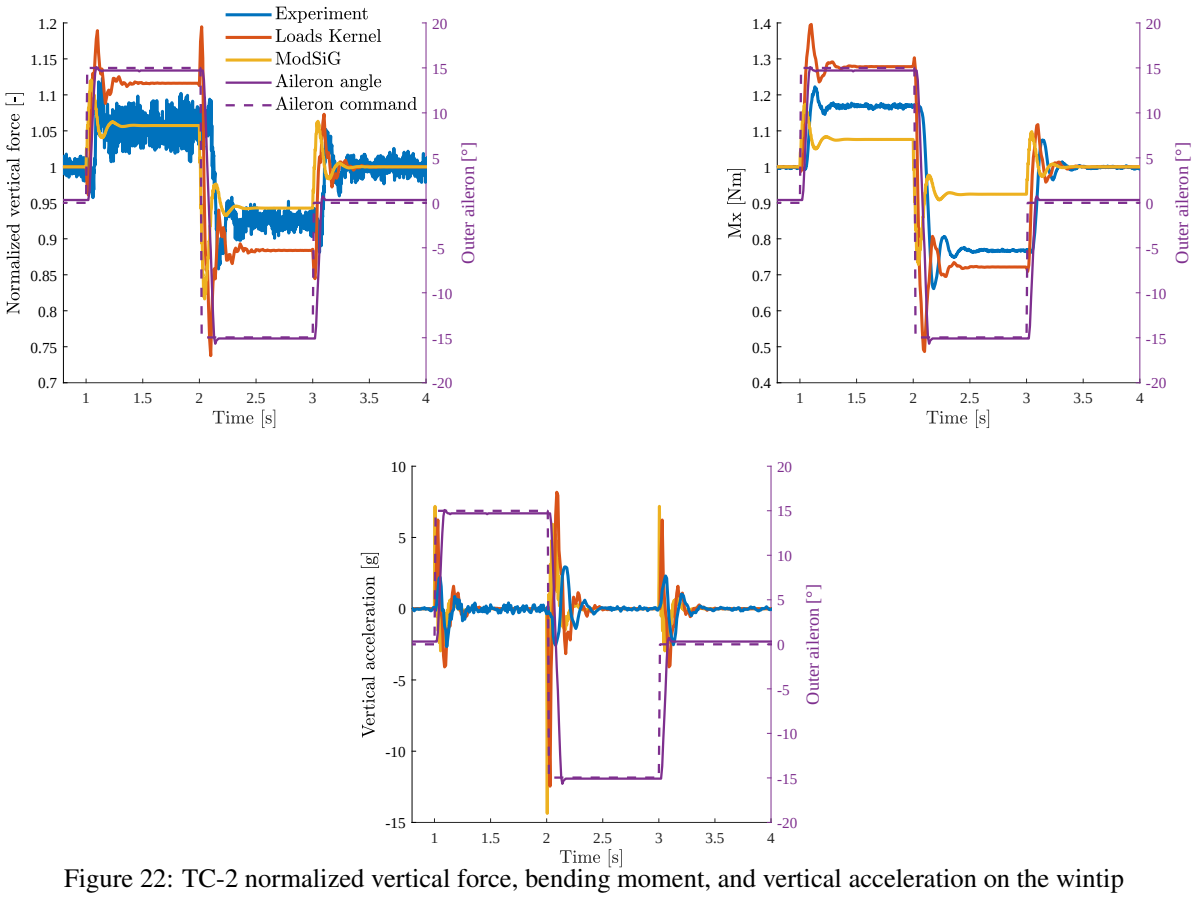

Figure 22: TC-2 normalized vertical force, bending moment, and vertical acceleration on the wintip

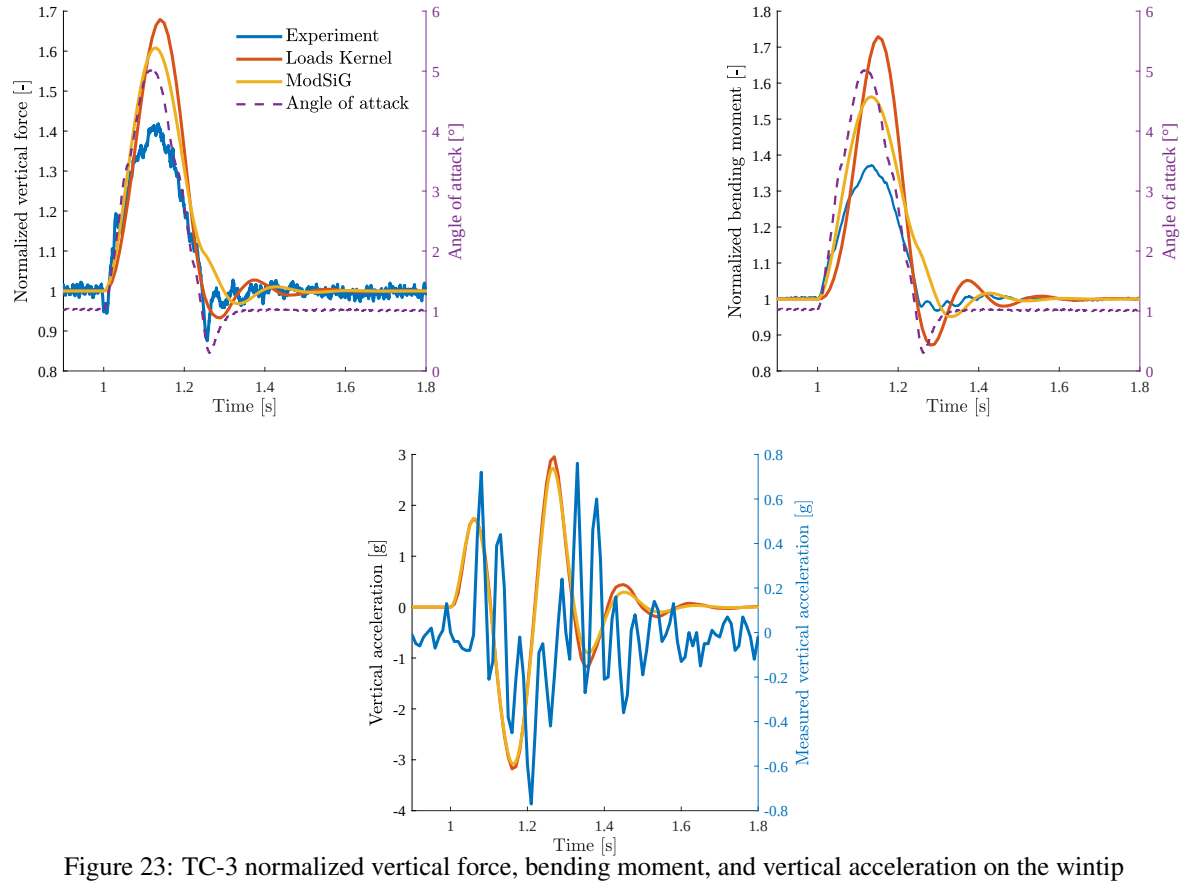

Figure 23: TC-3 normalized vertical force, bending moment, and vertical acceleration on the wintip

response in the acceleration not present in both models.

4.4 Conclusions

A step-by-step process to gather data for the validation of flexible wing models was proposed and applied in this paper. It is based on a bottom-to-top complexity approach. The process starts with data gathering for the validation of the stiffness properties of the wing. This is achieved by means of a static wing load test. This test allowed the identification of the stiffness matrix of the wing and to find the limits of the linear behavior of the wing. Then, a GVT was proposed to obtain the dynamic properties of the wing structure. This test allows for validating the dynamic analysis of the FEM. The natural frequencies and mode shapes of the structure were measured in a controlled environment and in the wind tunnel rig. These results characterize the structure's basic dynamic behavior and indicate how the structure will respond to dynamic loads. Lastly, a wind tunnel test campaign was performed to extract data to validate the aerodynamic model and the aeroelastic model of the wing. This bottom-to-top approach allows us to gradually tune the model from the structural to the aeroelastic model.

The process was applied to the TU-Flex FW. This wing was designed to fit all the facilities involved in this test campaign. The static results showed a good correlation between the simulation and the measured displacements in the linear regime with an average error lower than 2%. The GVT tests allowed to measure the frequencies and mode shapes of the wing in a "rigid" rig and in the wind tunnel setup. It is possible to appreciate that the wind tunnel joiner does not have a major influence on the dynamic of the wing even though the frequencies are not exactly the same. It was also possible to measure the motor/joiner dynamics. These dynamics could also be included in future models to add this boundary condition. The GVT allowed to measure the shapes and frequencies of the first eight modes of the wing with a good correlation between all identified and simulated modes, as demonstrated by the MAC. The larger error in the dynamic model was not in the shape but in the frequency of the first torsional mode. Further tests need to be performed to tune the torsional stiffness of the wing model. Nevertheless, there is a high level of similarity between the simulated modes and the constructed wing.

The first comparison between the experimental data and the models used to design the wing and the experiments show that the models are capable of following the correct wing trend. The general dynamics behavior is well represented by the models and the AoA and aileron input have the expected influence in the wing. Nevertheless, as expected for an untuned model the magnitudes for the forces and moments need further adjustments. The data collected will allow the estimation of the real wing polar, control surfaces efficiency, and the adjustment of the aeroelastic models.

The proposed approach is part of the initial validation process of the TU-Flex demonstrator. This campaign is the first in a series of multiple validation campaigns to tune the aeroelastic models and the controllers before they are installed in the flying demonstrators.

ACKNOWLEDGEMENTS

This study was financed in part by the German Federal Ministry for Economic Affairs and Climate Action (BMWK) due to a resolution of the German Federal Parliament within the scope of the LuFo VI-2 project FlexFuture (Grant number 20E2120A). The authors acknowledge the Load Analysis and Design, and the Aeroelastic Experiments Departments of the DLR for their support and contributions in carrying out this campaign. The authors acknowledge Martin Weberschock (Weberschock Development) for their commitment and support throughout the

construction process of the wing, and the technicians of TU-Berlin Institute of Aeronautics and Astronautics for their important contributions in the construction process of the wing joiner. To Carlos E. S. Cesnik for his important advice in the aircraft design review. To Christine Balder and the other FMRA and DLR-AE researchers and students who supported this wing's design and construction.

5 REFERENCES

[1] Palacios, R. and Cesnik, C. E. (2023). *Dynamics of Flexible Aircraft*. Cambridge University Press. doi:https://doi.org/10.1017/9781108354868.

[2] Drewiacki, D., Silvestre, F. J., and Guimarães Neto, A. B. (2019). Influence of airframe flexibility on pilot-induced oscillations. *Journal of Guidance, Control, and Dynamics*, 42(7), 1537–1550. doi:https://doi.org/10.2514/1.G004024.

[3] Silvestre, F. J., Guimarães Neto, A. B., Bertolin, R. M., et al. (2017). Aircraft control based on flexible aircraft dynamics. *Journal of Aircraft*, 54(1), 262–271. doi:https://doi.org/10.2514/1.C033834.

[4] González, P. J., Silvestre, F. J., Pereira, M. d. F. V., et al. (2020). Loop-separation control for very flexible aircraft. *AIAA Journal*, 58(9), 3819–3834. doi:https://doi.org/10.2514/1.J058692.

[5] Su, W. and Cesnik, C. E. (2010). Nonlinear aeroelasticity of a very flexible blended-wing-body aircraft. *Journal of Aircraft*, 47(5), 1539–1553. doi:https://doi.org/10.2514/1.47317.

[6] Deskos, G., del Carre, A., and Palacios, R. (2020). Assessment of low-altitude atmospheric turbulence models for aircraft aeroelasticity. *Journal of fluids and structures*, 95. doi:https://doi.org/10.1016/j.jfluidstructs.2020.102981.

[7] Ribeiro, F. L. C., Paglione, P., da Silva, R. G. A., et al. (2012). Aeroflex: a toolbox for studying the flight dynamics of highly flexible airplanes. In *7th International Congress of Mechanical Engineering, CONEM*.

[8] Banneheka Navaratna, P. D., Pontillo, A., Rezgui, D., et al. (2024). Wind tunnel investigations of a pitch-free flexible high aspect ratio aircraft model. In *AIAA SCITECH 2024 Forum*. p. 2819. doi:https://doi.org/10.2514/6.2024-2819.

[9] Drachinsky, A. and Raveh, D. E. (2020). Modal rotations: A modal-based method for large structural deformations of slender bodies. *AIAA Journal*, 58(7), 3159–3173. doi:https://doi.org/10.2514/1.J058899.

[10] Waszak, M. R. and Schmidt, D. K. (1988). Flight dynamics of aeroelastic vehicles. *Journal of Aircraft*, 25(6), 563–571. doi:https://doi.org/10.2514/3.45623.

[11] Hofstee, J., Kier, T., Cerulli, C., et al. (2003). A variable, fully flexible dynamic response tool for special investigations (varloads). In *IFASD 2003 - International Forum on Aeroelasticity and Structural Dynamics, Amsterdam, Netherlands*. doi:https://elib.dlr.de/12206/.

[12] Voß, A. (2020). *Design and structural optimization of a flying wing of low aspect ratio based on flight loads*. Doctoral thesis, Technische Universität Berlin, Berlin. doi:10.14279/depositonce-9858.

[13] Guimarães Neto, A. B., Barbosa, G. C., Paulino, J. A., et al. (2023). Flexible aircraft simulation validation with flight test data. *AIAA Journal*, 61(1), 285–304. doi:https://doi.org/10.2514/1.J060960.

[14] Quesada, A. A. G., González, P. J., Barbosa, G. C., et al. (2024). Influence of nonlinear aerodynamic effects on high aspect ratio aircraft model. In *IFASD 2024 - International Forum on Aeroelasticity and Structural Dynamics, Madrid, Spain*.

[15] Herrmann, B., Theis, J., and Thielecke, F. (2023). Nonlinear system identification of a uav model with distributed aerodynamics and flexible structure. *CEAS Aeronautical Journal*, 14(3), 661–677. doi:https://doi.org/10.1007/s13272-023-00674-x.

[16] Cesnik, C. E. S., Senatore, P. J., Su, W., et al. (2012). X-hale: A very flexible unmanned aerial vehicle for nonlinear aeroelastic tests. 50(12), 2820–2833. doi:https://doi.org/10.2514/1.J051392.

[17] Roessler, C., Stahl, P., Sendner, F., et al. (2019). Aircraft design and testing of flexop unmanned flying demonstrator to test load alleviation and flutter suppression of high aspect ratio flexible wings. In *Proceedings*, AIAA 2019-1813. AIAA Scitech 2019 Forum, San Diego, California: AIAA. doi:10.2514/6.2019-1813.

[18] Soal, K., Volkmar, R., Thiem, C., et al. (2023). Flight vibration testing of the t-flex uav using online modal analysis. In *AIAA SCITECH 2023 Forum*. p. 0373.

[19] Meddaikar, Y. M., Kier, T. M., Bartasevicius, J., et al. (2023). Aeroservoelastic induced drag modelling and minimization for the t-flex demonstrator. In *AIAA Scitech 2023 Forum*. doi:https://doi.org/10.2514/6.2023-0373.

[20] Drachinsky, A., Avin, O., Raveh, D. E., et al. (2022). Flutter tests of the pazy wing. *AIAA Journal*, 60(9), 5414–5421. doi:https://doi.org/10.2514/6.2022-2186.

[21] Hilger, J. and Ritter, M. R. (2021). Nonlinear aeroelastic simulations and stability analysis of the pazy wing aeroelastic benchmark. *Aerospace*, 8(10), 308. doi:https://doi.org/10.3390/aerospace8100308.

[22] Pereira, M. F., Chaves, G. B., Bertolin, R. M., et al. (2022). Experimental validation of model predictive controllers for load alleviation in very flexible aircraft. In *IFASD 2022 - International Forum on Aeroelasticity and Structural Dynamics, Madrid, Spain*.

[23] Ricci, S., De Gaspari, A., Riccobene, L., et al. (2017). Design and wind tunnel test validation of gust load alleviation systems. In *58th AIAA/ASCE/AHS/ASC Structures, Structural Dynamics, and Materials Conference*. p. 1818. doi:https://doi.org/10.2514/6.2017-1818.

[24] Heaney, P. S. and Quindlen, J. F. (2024). Overview of the integrated adaptive wing technology maturation wind-tunnel test objectives. In *AIAA SCITECH 2024 Forum*. p. 2509. doi:https://doi.org/10.2514/6.2024-2509.

[25] González, P. J., Stavorinus, G., Silvestre, F. J., et al. (2023). Tu-flex: A very-flexible flying demonstrator with a generic transport aircraft configuration. In *AIAA SCITECH 2023 Forum*. doi:https://doi.org/10.2514/6.2023-1312.

[26] González, P. J., Shahi, H., Meddaikar, Y. M., et al. (2022). Flexible-wing design process for tu-flex demonstrator. In *IFASD 2022 - International Forum on Aeroelasticity and Structural Dynamics, Madrid, Spain*.

[27] González, P. J., Stavorinus, G., Shahi, H., et al. (2022). A preliminary structural design of a flexible flying demonstrator. In *ICAS 2022 - 33rd Congress of the International Council of the Aeronautical Sciences, Stockholm, Sweden*. ISSN 2958-4647.

[28] Fragner, M., Weinman, K., Deiterding, R., et al. (2014). Numerical and experimental studies of train geometries subject to cross winds. In *"Proceedings of the Second International Conference on Railway Technology: Research, Development and Maintenance", Civil-Comp Press,*. doi:doi:10.4203/ccp.104.24.

[29] Klimmek, T. (2014). Parametric set-up of a structural model for fermat configuration aeroelastic and loads analysis. *Journal of Aeroelasticity and Structural Dynamics*, 3(2). doi:10.3293/asdj.2014.27.

[30] Klimmek, T. (2009). Parameterization of topology and geometry for the multidisciplinary optimization of wing structures. In *CEAS 2009 - European Air and Space Conference*. doi:https://elib.dlr.de/65746/.

[31] Sousa Vicente, F. (2019). Stacking sequence retrieval of large composite structures in bi-step optimization strategies using mechanical constraints. *Master Thesis - TU-Delft*.

[32] Voß, A. (2020). Loads kernel user guide. Tech. Rep. DLR-IB-AE-GO-2020-136, German Aerospace Center (DLR). Https://elib.dlr.de/140268/.

[33] Voß, A. (2020). An implementation of the vortex lattice and the doublet lattice method. Tech. Rep. DLR-IB-AE-GO-2020-137, German Aerospace Center (DLR). Https://elib.dlr.de/136536/.

[34] Barbosa, G. C., Quesada, A. A. G., González, P. J., et al. (2024). Aeroservoelastic analysis and load alleviation control for very flexible aircraft: Tu-flex study. In *IFASD 2024 - International Forum on Aeroelasticity and Structural Dynamics, Madrid, Spain*.

[35] Silvestre, F. J. and Luckner, R. (2015). Experimental validation of a flight simulation model for slightly flexible aircraft. *AIAA Journal*, 53(12), 3620–3636. doi:10.2514/1.J054023.

[36] Ritter, M., Dillinger, J., and Meddaikar, Y. M. (2017). Static and dynamic aeroelastic validation of a flexible forward swept composite wing. In *58th AIAA/ASCE/AHS/ASC structures, structural dynamics, and materials conference*. doi:https://doi.org/10.2514/6.2017-0637.

[37] Allemang, R. J. (1982). A correlation coefficient for modal vector analysis. In *Proceedings of the 1st International Modal Analysis Conference, Orlando, USA*.

COPYRIGHT STATEMENT